Meta-Radiology 2 (2024) 100101

Contents lists available at ScienceDirect

Meta-Radiology

journal homepage: www.keaipublishing.com/en/journals/meta-radiology

Original Article

Evaluation of cerebellar aging in MRI images: Fractal analysis compared to Euclidean geometry-based morphometry

Nataliia Maryenko *, Oleksandr Stepanenko

Department of Histology, Cytology and Embryology, Kharkiv National Medical University, Kharkiv, Ukraine

ARTICLE INFO

Keywords:
Aging
Cerebellum
Fractals
Morphometry
MRI
Texture analysis

ABSTRACT

Objectives: This study aimed to identify age-related changes in the fractal dimensions of the cerebellum and compare the sensitivity of fractal analysis and conventional Euclidean geometry-based morphometry to cerebellar aging.

Material and methods: Two-dimensional T2-weighted magnetic resonance images from the brains of 100 conditionally healthy individuals (44 males and 56 females) aged 18–86 years were examined, with a focus on midsagittal sections of the cerebellar vermis. We determined ten parameters derived from Euclidean geometry (perimeter, area, and indices calculated from them), along with seven fractal dimension values derived from fractal geometry (the approximated fractal dimensions of the overall cerebellar tissue, white matter, overall cerebellar cortex and its granular and molecular layers, outer contour, and digital skeleton).

Results: Fractal dimensions demonstrated stronger correlation relationships with age compared to morphometric parameters derived from Euclidean geometry. The most pronounced age-related declines were observed in the approximated fractal dimensions of the cerebellar cortex and its layers, with decreases also noted in the fractal dimensions of the outer contour and digital cerebellar skeleton. Fractal dimension values did not significantly differ between males and females, while several Euclidean geometry-derived parameters showed sexual dimorphism. Although males demonstrated stronger relationships of some studied parameters with age, there was no statistically significant difference in the sex-related dynamics of aging.

Conclusion: The normal aging of the cerebellum involves not only absolute size alterations but also changes in the texture and spatial configuration of cerebellar tissue components, which can be quantitatively and objectively assessed by fractal analysis.

1. Introduction

The cerebellum, or "little brain," despite its name, makes a significant contribution to the functioning of the nervous system. For a long time, the cerebellum was considered merely as the center for coordinating movements, maintaining body balance and spatial navigation. However, research in recent decades has demonstrated the involvement of the cerebellum in cognition and emotional regulation.[1,2] The importance of these cerebellar functions is underscored by the impact of age-related changes on the development not only of coordination and balance disorders associated with aging but also on age-related cognitive dysfunction.[3–6] Considering the influence of age-related changes on cerebellar function, a crucial task is to assess the structural changes observed during normal aging, which serve as the morphological basis for age-related decline in cerebellar function.

Modern neuroimaging techniques, particularly Magnetic Resonance Imaging (MRI), are highly informative and applicable for the in vivo detection of morphological changes in the cerebellum during normal aging and various pathological conditions.[7,8] MRI offers significant advantages in the study of cerebellar aging due to its non-invasive nature and high spatial resolution.[8–10] It allows for detailed visualization of cerebellar structures, enabling precise measurement of morphometric parameters.[9,10]

Structural MRI has proven to be sufficiently informative for detecting and characterizing cerebellar changes in both normal aging[7,8] and in identifying specific cerebellar alterations.[11–16] Recent studies have

* Corresponding author. Department of Histology, Cytology and Embryology, Kharkiv National Medical University, Kharkiv, 4 Nauky avenue, 61022, Ukraine.
E-mail addresses: maryenko.n@gmail.com, ni.marienko@knmu.edu.ua (N. Maryenko), oy.stepanenko@knmu.edu.ua (O. Stepanenko).
Peer review under the responsibility of Editorial Board of Meta-Radiology.

https://doi.org/10.1016/j.metrad.2024.100101
Received 5 May 2024; Received in revised form 29 August 2024; Accepted 2 September 2024
Available online 4 September 2024

highlighted the potential involvement of the cerebellum in neurodegenerative diseases, including Alzheimer's disease, Parkinson's disease, multiple sclerosis, small vessel disease and vascular dementia.[11,12] These conditions can be considered forms of pathological brain aging, necessitating the development of diagnostic criteria to distinguish them from normal aging. Additionally, acquired and congenital ataxias of various etiologies exhibit structural changes in MRI images of cerebellum and may mimic the changes observed in normal cerebellar aging.[13–16] This underscores the utility of MRI in assessing cerebellar structure and detecting both specific and nonspecific cerebellar changes.

Structural studies related to the examination of the cerebellum during aging typically rely on morphometric methods derived from Euclidean ("classical") geometry. In various studies, age-associated changes (typically reductions) in various parameters have been identified, including changes in linear dimensions,[17,18] cross-sectional area of cerebellar vermis and its lobules,[18–20] as well as volumes of the cerebellar vermis, vermal and hemispheric lobules, along with volumes of cerebellar gray and white matter.[21–24]

The alternative method that can be utilized to evaluate the spatial configuration's peculiarities of the cerebellum is fractal geometry.[25] Unlike Euclidean geometry, fractal geometry provides a quantitative assessment not of absolute sizes but of the degree of space filling, characterized by a parameter known as fractal dimension.[25] As the complexity of the spatial configuration of the studied structure increases (e.g., increased folding of the cerebral or cerebellar cortex), the degree of space filling by the studied structure rises, and consequently, its fractal dimension increases. Therefore, fractal dimension can be considered a measure of the structural complexity and the intricacy of the spatial configuration of the studied objects. Fractal analysis, the research method identifying fractal dimension, is quite informative for the studies of the structures and objects that have fractal properties – self-similarity, scale invariance, a high number of similar details, etc.[25]

Among the brain structures, the cerebral hemispheres are the most "popular" object for fractal analysis. Among the extensive body of work that involved conducting fractal analysis on cerebral hemispheres, several studies stand out where fractal analysis has been successfully applied to detect and quantitatively characterize changes associated with normal aging[26–30] or neurodegeneration, including studies regarding multiple sclerosis,[31,32] and Alzheimer's disease.[33,34]

The cerebellum, despite its intricate configuration, has less frequently been the object of fractal analysis, with only a few studies employing fractal analysis to investigate it.[35–43] Authors have identified changes in the fractal dimensions of the cerebellar cortex and white matter in conditions such as multiple system atrophy of the cerebellar type,[38] Chiari malformation,[39–41] spinocerebellar ataxia type 2,[42] and autism spectrum disorder.[43] However, the investigations on cerebellar aging using fractal analysis of MRI brain scans appear to be lacking in the available literature. Therefore, in this study, we aimed to identify age-related changes in the fractal dimensions of the cerebellum and to compare the sensitivity of fractal analysis and conventional Euclidean geometry-based morphometry to cerebellar aging. By exploring these methodologies, we sought to determine their potential as diagnostic tools for detecting early cerebellar changes that could precede clinical symptoms, thereby offering a new avenue for the early diagnosis and differentiating of cerebellar changes in normal aging from cerebellar degeneration in pathological conditions.

In our earlier studies, which were based on a smaller sample size (N = 30, aged 18–30 years), we primarily focused on determining the fractal dimensions of overall cerebellar tissue, its linear contours, and digital skeletons using preliminary methodology.[44,45] The present study was designed for a comprehensive analysis of age-related changes in fractal dimensions. To achieve this, we significantly expanded both the sample size (N = 100, aged 18–86 years) and the scope of the analysis. We modified and further developed our fractal analysis methods and image preprocessing techniques, enabling the exploration of seven distinct fractal dimensions of cerebellar tissue in two-dimensional MRI images. Additionally, this study incorporates a comprehensive set of Euclidean geometry-based morphometric parameters alongside fractal dimensions, allowing for a detailed examination of age-related changes, sex differences, and correlations between these parameters, which were not studied in detail in our previous studies or in the studies by other researchers.

2. Material and methods

2.1. Participants of the study

As research material, MRI images of the brains of 100 conditionally healthy individuals (44 males and 56 females) were utilized. We reused a sample from our previous investigation into fractal analysis of cerebral hemispheres.[46] The participants of the study underwent magnetic resonance brain imaging for diagnostic purposes, and since no pathological structural changes in the brain and surrounding tissues were detected, these individuals were considered conditionally healthy, with the brain structure deemed conditionally normal.

The age of the study participants ranged from 18 to 86 years. The demographic data of the sample is presented in Table 1. The mean ranks of age values between males and females were not significantly different ($p = 0.811$), as determined by the Mann-Whitney *U* test. Furthermore, the distribution of age values within the male and female groups was also not significantly different ($p = 0.920$), as determined by the Kolmogorov-Smirnov KS test.

2.2. MRI protocol

The brain scanning was performed using a Siemens Magnetom Symphony MRI scanner with a magnetic induction value of 1.5 T. T2-weighted images were examined. The MRI parameters were as follows: echo time (TE) 122 ms, repetition time (TR) 4520 ms, and a slice thickness 5 mm. The digital MRI images had a resolution of 72 pixels per inch, and the absolute scale was 3 pixels = 1 mm.

To ensure the reliability and accuracy of the MRI data, several quality control measures were implemented throughout the imaging process. Before the acquisition of MRI images, scanner calibration was performed to verify consistent imaging performance. All MRI images underwent rigorous inspection for head tilt, motion and interference artifacts, and those with excessive heal tilt, motion and interference due to dental prosthetics were excluded from the analysis. Additionally, the consistency of the imaging protocol was maintained across all sessions, with careful attention to parameters such as slice thickness, field of view, and acquisition time, thereby minimizing variability. Lastly, an experienced radiologist reviewed the images to ensure anatomical accuracy and proper alignment, ensuring that only high-quality images were included in the study.

2.3. Region of interest

The region of interest in the present study is the cerebellar vermis, specifically the midsagittal MRI image intercepting the cerebellar vermis region. According to the principle of mediolateral continuity,[47] the lobules and fissures of the cerebellum in both hemispheres and vermis exhibit structural continuity. The configuration and structure of the cerebellar vermis in its mid-sagittal section reflect the characteristics of

Table 1
Demographic data of the study participants.

Age range, years	Number of participants		
	Total	Males	Females
18–30	31	14	17
31–45	29	14	15
46–60	24	8	16
61–86	16	8	8
Total	100	44	56

both hemispheres. This makes it a representative and integral part of the cerebellum's anatomy. Additionally, the midsagittal section of the cerebellar vermis is uniform across all MRI sequences and its localization is consistent among individuals, minimizing variability. In contrast, the cerebellar hemispheres can vary in size and shape, making it challenging to standardize the MRI slices representing the same hemispheric regions across different individuals. By focusing on the midsagittal section of the cerebellar vermis, we aimed to ensure standardization and reduce potential bias arising from individual anatomical differences.

2.4. Algorithm of image preprocessing and morphometric analysis

2.4.1. Transfer of MRI images for further processing in a graphics editor

For image preprocessing, the Adobe Photoshop CS5 graphics editor was utilized. Using this software, blank frame JPEG images with dimensions of 160 × 160 pixels and a resolution of 128 pixels per inch were created. Subsequently, a fragment of the digital MRI DICOM image containing the entire midsagittal section of the cerebellum was copied and pasted into the previously created frame JPEG image (all pixels were copied and pasted as they are, without scaling at this stage). The placement of the MRI image fragment ensured that the region corresponding to the cerebellar vermis did not extend beyond the boundaries of the created image frame (Fig. 1).

2.4.2. Image scaling

After placing the copied fragment, the parameters of the newly created image were adjusted: its dimensions were increased from 160 × 160 pixels to 360 × 360 pixels, resulting in an increase in resolution from 128 pixels per inch to 288 pixels per inch (Fig. 1). As a result, the absolute scale of the image increased from 3 pixels = 1 mm to 6.75 pixels = 1 mm, and the absolute image area intercepted by each individual pixel, decreased from 0.111 mm^2 to 0.022 mm^2. In our previous works,[44,45] we did not perform scaling during image preprocessing for fractal analysis.

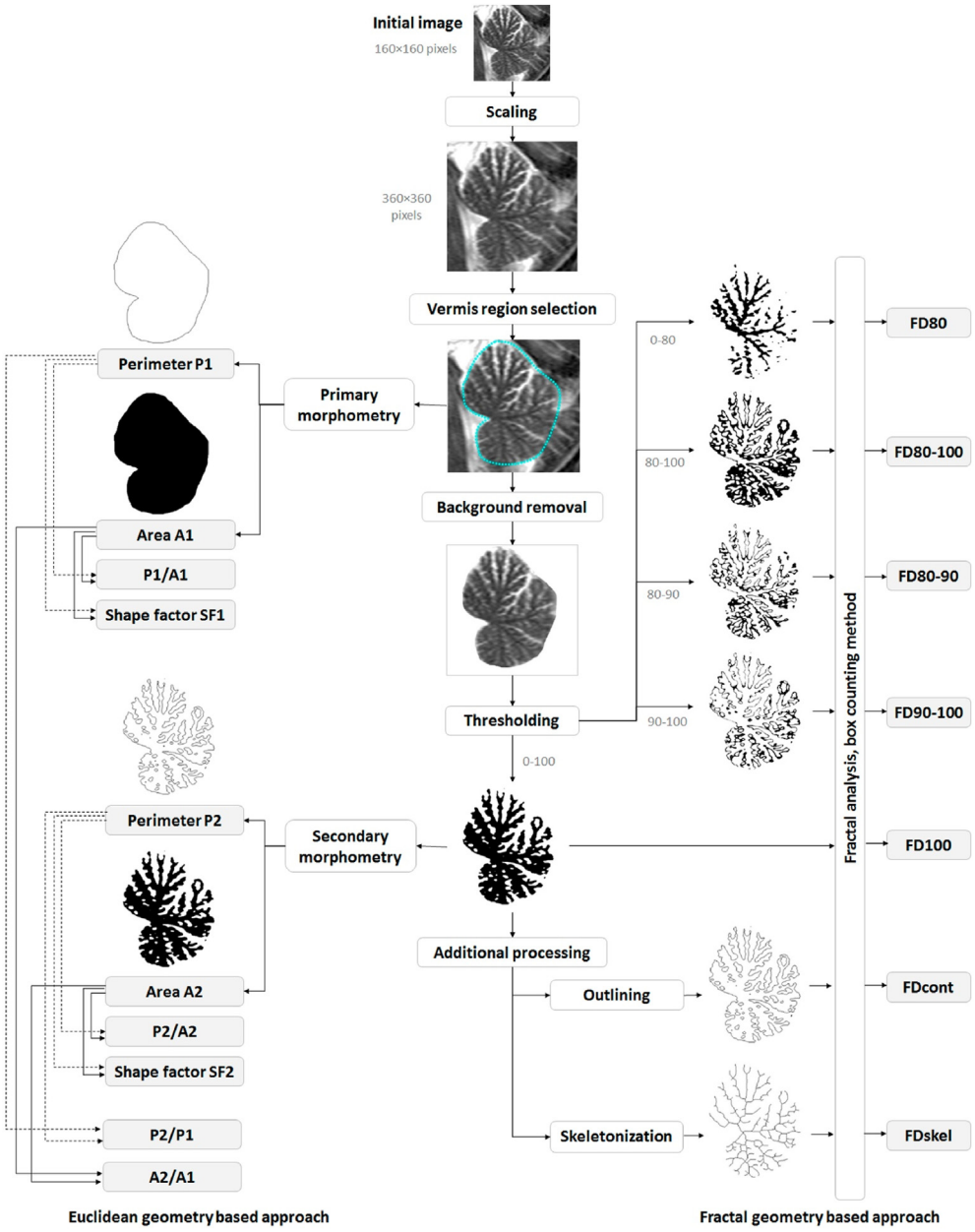

Fig. 1. Algorithm for the preprocessing and morphometric analysis of MRI images of the cerebellum to detect and characterize age-related changes: approaches based on Euclidean and fractal geometries.

During the development of the methodology for this study, we attempted additional segmentation of MRI images using different intensity threshold values to approximate the identification of various components of cerebellar tissue (see subsection 2.4.6). However, the primary results were unsatisfactory: the masks for the cerebellar cortex were discontinuous, consisting of individual pixels and broken lines, and did not accurately represent the actual convolutions of the cortex (Fig. 2A). This issue can be attributed to the small thickness of the cerebellar cortex and its individual layers. To enhance the quality of the images, we attempted to artificially increase their dimensions. The scaling procedure reduced the size of each pixel, allowing the layers of the cerebellar cortex to be represented as continuous lines (Fig. 2B). Bicubic interpolation was used for scaling.

2.4.3. Selection of the cerebellar vermis region and primary morphometry

In the next stage, the region corresponding to the cerebellar vermis was manually selected according to the external surface of the cerebellum. The "selection" tool in Adobe Photoshop CS5 was used for this purpose. During this process, fragments of the cerebellar tonsils, which may be present in some individuals in the midsagittal tomographic section due to individual anatomical variability, were not included in the selected region. Since the cerebellar tonsils belong to the cerebellar hemispheres (lobule IX), we chose to focus only on the vermal lobules for analysis. After selecting the cerebellar vermis region, initial morphometry was immediately conducted, measuring the perimeter and area (perimeter P1 and area A1). The "analysis" tool in Adobe Photoshop CS5 was used for measurements.

2.4.4. Image segmentation: revealing the overall cerebellar tissue and secondary morphometry

After selecting the cerebellar vermis region, the background was removed. The selected area was inverted, and the background pixels were filled with a white color (pixel intensity of 255) (Fig. 1).

The subsequent step involved image segmentation with conversion to a binary format (i.e., an image consisting only of black and white pixels – corresponding to pixel intensity of 0 and 255, respectively). To achieve this, the layer with the image obtained in the previous stage was duplicated, and segmentation was performed using the "threshold" tool in Adobe Photoshop CS5.

Initially, segmentation via thresholding was performed to identify pixels corresponding to the overall cerebellar tissue. We applied an empirical intensity threshold of 100. Following this segmentation, pixels with intensity equal to or less than 100 were assigned a black color, while brighter pixels were assigned a white color. The chosen threshold of 100 for segmentation allowed us to delineate the silhouette of the cerebellar tissue, revealing both the visible cerebellar pial surface and the pial surface hidden within the fissures between lobules and within them.

Subsequent to thresholding, the segmented area (all black-colored pixels) approximately corresponding to overall cerebellar tissue was selected, and using the "analysis" tool, the perimeter and area of this region were determined again (perimeter P2 and area A2). Thus, secondary morphometry was conducted (Fig. 1).

2.4.5. Morphometric parameters derived from Euclidean geometry

Alongside with the initial stages of image preprocessing using primary and secondary morphometry, the following morphometric parameters derived from Euclidean geometry were determined (Fig. 1):

- Perimeter P1, corresponding to the length of the contour of the visible cerebellar pial surface.
- Area A1, corresponding to cerebellar tissue, including the content of fissures and sulci.
- Perimeter P2, approximately corresponding to the length of the contour of the entire cerebellar pial surface (including the surface hidden within fissures and sulci).
- Area A2, approximately corresponding to cerebellar tissue excluding the content of fissures and sulci.

In addition to the four basic parameters, six additional indices were calculated:

- Perimeter-to-area ratio (P1/A1 and P2/A2).
- Shape factor, or circularity (SF1 and SF2). SF was determined by the formula ($SF = (4\pi \times A)/P^2$).[48]
- Perimeter ratio (P2/P1), a two-dimensional gyrification index.
- Area ratio (A2/A1).

2.4.6. Image segmentation: revealing the components of cerebellar tissue and additional image processing

The next step in image preprocessing involved multiple thresholding to reveal cerebellar tissue components for fractal analysis. The individual components of cerebellar tissue have different densities and, consequently, different pixel intensities in MRI images. This allowed us to perform image preprocessing using thresholding cocreate binary masks of cerebellar tissue components. In addition to segmentation with an intensity threshold of 100, images were also segmented with a threshold value of 80, revealing the deepest and densest areas of the cerebellar branches – these areas approximately

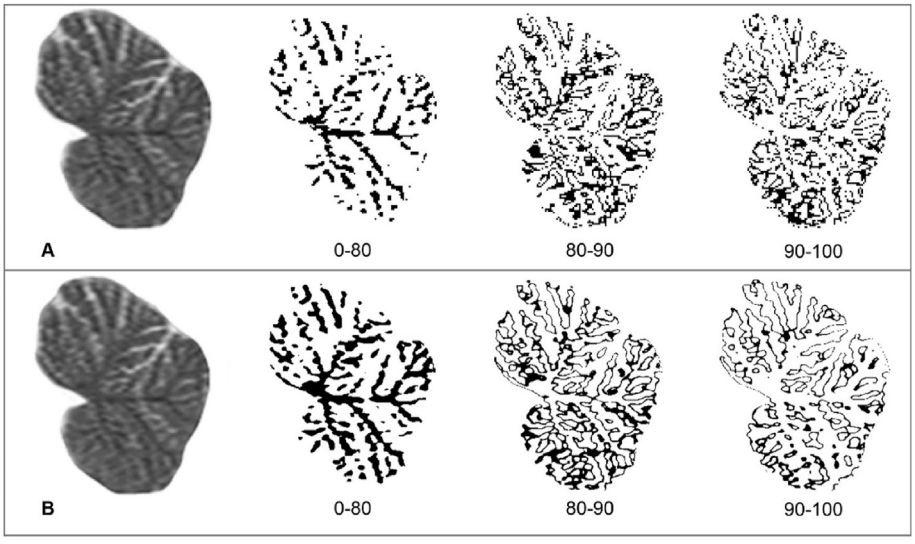

Fig. 2. Thresholding of the non-scaled MRI image (A) and the MRI image after scaling (B), revealing the components of cerebellar tissue: white matter (0–80), granular layer of the cerebellar cortex (80–90), and molecular layer of the cerebellar cortex (90–100). In the non-scaled image, the contours of the masks for the granular and molecular layers are discontinuous due to the thickness of these layers being smaller than the pixel size. Scaling reduces the area intercepted by a single pixel, thereby minimizing discontinuity in the cerebellar cortex masks.

correspond to the localization of white matter. Therefore, the fractal dimension determined from such images can be considered an approximated fractal dimension of the cerebellar white matter. Additionally, images were thresholded in the intensity range of 80–100 (the difference between the two previous thresholding results), thus identifying areas corresponding to the cerebellar cortex. The fractal dimension determined from such images can be considered an approximated fractal dimension of the cerebellar cortex. Further segmentation was performed in the range of 90–100 (regions corresponding to the molecular layer of the cerebellar cortex) and 80–90 (regions corresponding to the granular layer of the cerebellar cortex).

Additionally, besides thresholding based on intensity values, outlining and skeletonization of the silhouettes obtained during segmentation with a threshold of 100 were carried out. For this purpose, the "outline" and "skeletonize" tools of the Image J software (Fiji package)[49] were utilized. The thickness of the lines of the digital skeleton and linear contour was set to 1 pixel.

2.4.7. Fractal analysis and parameters derived from fractal geometry

After preprocessing, a fractal analysis was conducted using the classical "box counting" method.[50] For this purpose, the "fractal box count" tool in the Image J (Fiji) software[49] was employed. This method was applied to all image segmentation variants described above. We utilized 6 stages of fractal analysis with the following BoxSize values: 2 pixels, 4 pixels, 8 pixels, 16 pixels, 32 pixels, and 64 pixels. Thus, seven fractal dimension (Minkowski dimension) values were determined (Fig. 1):

- FD100 – fractal dimension determined on silhouette images obtained during thresholding in the intensity range of 0–100. *An approximated fractal dimension of overall cerebellar tissue.*
- FD80 – fractal dimension determined on images obtained during thresholding in the intensity range of 0–80. *An approximated fractal dimension of cerebellar white matter.*
- FD80-100 – fractal dimension determined on images obtained during thresholding in the intensity range of 80–100. *An approximated fractal dimension of the overall cerebellar cortex.*
- FD80-90 – fractal dimension determined on images obtained during segmentation in the intensity range of 80–90. *An approximated fractal dimension of the granular layer of the cerebellar cortex.*
- FD90-100 – fractal dimension determined on images obtained during segmentation in the intensity range of 90–100. *An approximated fractal dimension of the molecular layer of the cerebellar cortex.*
- FDcont – fractal dimension of outlined contour.
- FDskel – fractal dimension of skeletonized images.

2.5. Statistics

Statistical data processing was carried out using Microsoft Excel 2016. The following statistical parameters were calculated: arithmetic mean (M), standard deviation (σ), median (Me), 25th and 75th percentiles (Q1 and Q3, respectively), minimum (min), and maximum (max) values. The normality of the value distribution was assessed using the Shapiro-Wilk W test. The Kruskal-Wallis H test with post-hoc Dunn's test and Bonferroni adjustment for multiple comparisons was employed to compare fractal dimension values. Mann-Whitney *U* test was used to assess sex differences. Kolmogorov-Smirnov KS test was employed to assess difference between age distributions in males and females. Fisher F test was used to compare linear regression equations characterizing the age dynamics of the studied parameters in males and females. As some studied parameters had a value distribution differing from normal, a non-parametric Spearman's rank correlation coefficient (R) was calculated to determine relationships between obtained values, and its significance was evaluated using Student's *t*-test. The level of statistical significance was set at $\alpha = 0.05$.

3. Results

3.1. Descriptive statistics of morphometric parameters of the cerebellar vermis

The descriptive statistical data characterizing the values of the studied parameters are presented in Table 2. After examining the distribution of values, it was found that most parameters exhibited a normal distribution. However, some parameters had a distribution of values that significantly differed from normal.

The values of parameters derived from Euclidean geometry, determined using primary and secondary morphometry, significantly differed from each other. Specifically, the value of perimeter P2, corresponding to the length of the entire pial surface, was nearly three times larger than the value of perimeter P1. Therefore, the mean value of the two-dimensional gyrification index (P2/P1) was close to 3. However, it should be noted that this study utilized MRI images which have limited structural detailing; it may lead to the underestimation of P2 values (due to smoothing of the surface) and lower gyrification index values compared to real values. Additionally, it should be noted that area A2 (approximated cross-sectional area of the overall cerebellar tissue) can differ from the real cross-sectional area of cerebellar tissue due to segmentation of the MRI images with limited resolution.

When comparing values of fractal dimension among themselves, the null hypothesis of no differences was rejected ($p < 0.001$). Subsequent pairwise multiple comparisons revealed that the vast majority of fractal dimension values significantly differed from each other ($p < 0.001$), with the exception of FD80 and FD80-90 ($p = 0.370$).

3.2. Morphometric parameters of the cerebellar vermis in males and females

When comparing the values of the studied parameters between males and females (Table 2), it was found that the majority of values did not significantly differ. However, statistically significant differences were identified in parameters derived from Euclidean geometry, specifically perimeters P1 and P2, which accounted for differences in both shape factors (SF1 and SF2), the gyrification index (P2/P1), and the perimeter-to-area ratio (P2/A2). Nevertheless, both area values in males and females did not significantly differ, although the mean and median area values were slightly higher in males. In the comparison of fractal dimension values, no statistically significant differences were found between males and females.

3.3. Correlation analysis: correlations between morphometric parameters of the cerebellar vermis

In the next stage of the study, a correlation analysis was conducted to determine the nature of relationships between the investigated parameters (Fig. 3). The majority of parameters derived from Euclidean geometry were strongly or moderately correlated with each other. Stronger correlations were identified among parameters determined using the same approach for determining perimeter and area values (primary or secondary morphometry): P1, A1, P1/A1, SF1, or P2, A2, P2/A2, SF2.

Fractal dimension values, except for FD80, positively correlated with each other. The strongest correlation relationships were demonstrated by the group of approximated fractal dimensions of the cortex and its individual layers (FD80-100, FD80-90, and FD90-100) along with FDcont and FDskel. It can be hypothesized that these values are influenced by similar factors, such as the number of gyri (folia) and the complexity of their shapes. This assumption can be supported by the close correlations of these fractal dimensions with perimeter values and the two-dimensional gyrification index (P2/P1), indirectly characterizing the convolutedness of the cerebellar cortex. Additionally, most of the studied parameters demonstrated weak to moderate correlations with both area values.

Table 2
Descriptive statistics of morphometric parameters of the cerebellar vermis.

Parameter	Sex group	M	SD	Min	Q1	Me	Q3	Max	p (SW test for normality)	p (*U* test for sex difference)
P1, cm	Total	14.174	0.797	12.600	13.592	14.133	14.667	16.400	0.014	0.027
	Males	14.334	0.741	13.000	13.717	14.383	14.742	16.300		
	Females	14.049	0.824	12.600	13.533	13.833	14.350	16.400		
A1, cm^2	Total	11.672	1.181	8.592	10.887	11.484	12.479	15.594	0.138	0.393
	Males	11.782	1.322	8.592	10.910	11.661	12.764	15.594		
	Females	11.587	1.062	8.856	10.842	11.451	12.417	14.707		
P1/A1	Total	1.221	0.081	1.024	1.151	1.224	1.258	1.521	0.005	0.992
	Males	1.226	0.095	1.043	1.146	1.224	1.267	1.521		
	Females	1.217	0.069	1.024	1.156	1.223	1.255	1.423		
SF1	Total	0.730	0.047	0.573	0.714	0.741	0.763	0.814	<0.001	0.008
	Males	0.719	0.045	0.604	0.695	0.732	0.748	0.779		
	Females	0.739	0.047	0.573	0.719	0.747	0.766	0.814		
P2, cm	Total	41.126	5.356	29.133	37.475	41.350	44.092	57.867	0.561	0.002
	Males	42.954	6.228	29.233	39.900	42.917	45.717	57.867		
	Females	39.689	4.068	29.133	37.117	39.267	42.175	48.033		
A2, cm^2	Total	6.967	0.936	4.576	6.290	6.912	7.602	10.063	0.725	0.674
	Males	7.004	0.947	4.680	6.262	6.987	7.581	10.063		
	Females	6.937	0.935	4.576	6.300	6.845	7.609	9.023		
P2/A2	Total	5.981	0.968	4.192	5.194	5.860	6.666	8.888	0.009	0.035
	Males	6.188	0.930	4.452	5.614	6.054	6.814	8.888		
	Females	5.819	0.975	4.192	5.100	5.684	6.329	8.409		
SF2	Total	0.054	0.014	0.026	0.044	0.054	0.061	0.097	0.148	0.004
	Males	0.050	0.014	0.026	0.043	0.048	0.057	0.097		
	Females	0.057	0.013	0.031	0.049	0.058	0.065	0.091		
P2/P1	Total	2.899	0.319	2.182	2.683	2.866	3.089	3.690	0.806	0.007
	Males	2.988	0.341	2.182	2.831	2.986	3.214	3.690		
	Females	2.829	0.284	2.213	2.646	2.782	3.026	3.523		
A2/A1	Total	0.597	0.052	0.491	0.560	0.599	0.634	0.700	0.174	0.854
	Males	0.595	0.052	0.492	0.559	0.596	0.633	0.694		
	Females	0.598	0.052	0.491	0.560	0.600	0.635	0.700		
FD100	Total	1.737	0.029	1.595	1.723	1.738	1.755	1.801	0.001	0.763
	Males	1.737	0.029	1.595	1.724	1.740	1.755	1.777		
	Females	1.738	0.029	1.644	1.723	1.736	1.755	1.801		
FD80	Total	1.570	0.059	1.442	1.532	1.573	1.608	1.707	0.609	0.674
	Males	1.573	0.059	1.442	1.545	1.573	1.611	1.705		
	Females	1.568	0.059	1.454	1.531	1.572	1.606	1.707		
FD80-100	Total	1.638	0.043	1.480	1.618	1.646	1.668	1.708	0.001	0.970
	Males	1.636	0.046	1.496	1.611	1.652	1.670	1.705		
	Females	1.640	0.040	1.480	1.619	1.644	1.668	1.708		
FD80-90	Total	1.554	0.041	1.395	1.532	1.557	1.577	1.640	0.006	0.629
	Males	1.549	0.045	1.395	1.529	1.557	1.580	1.617		
	Females	1.558	0.039	1.456	1.537	1.558	1.576	1.640		
FD90-100	Total	1.502	0.047	1.367	1.477	1.505	1.535	1.619	0.239	0.690
	Males	1.503	0.051	1.367	1.471	1.517	1.546	1.589		
	Females	1.502	0.044	1.382	1.480	1.504	1.523	1.619		
FDcont	Total	1.434	0.043	1.343	1.404	1.432	1.462	1.543	0.790	0.142
	Males	1.441	0.045	1.343	1.409	1.447	1.474	1.526		
	Females	1.429	0.041	1.352	1.399	1.428	1.452	1.543		
FDskel	Total	1.340	0.038	1.212	1.321	1.341	1.361	1.436	0.155	0.516
	Males	1.342	0.038	1.212	1.325	1.344	1.361	1.423		
	Females	1.339	0.039	1.239	1.319	1.337	1.361	1.436		

3.4. Correlation analysis: correlations between morphometric parameters of the cerebellar vermis and age

To identify the peculiarities of age-related changes in the cerebellum, we computed correlation coefficients between the studied parameters and age (Table 3). To eliminate the influence of absolute cerebellar sizes and their age dynamics on other parameters, the correlation coefficients normalized by the area A1 were additionally calculated.

Most of the Euclidean geometry-derived parameters showed weak to moderate negative correlations with age. In contrast, fractal dimension values demonstrated stronger correlations with age: most fractal dimensions had statistically significant correlations with age, except for FD100: the approximated fractal dimension of the overall cerebellar tissue (FD100) remained practically unchanged with age. However, changes were observed in individual components of cerebellar tissue. Specifically, FD80 (approximated fractal dimension of white matter) increased with age, while the approximated fractal dimensions of the cortex and its layers (FD80-100, FD80-90, and FD90-100), fractal dimension of cerebellar contour (FDcont) and digital skeletons (FDskel) decreased. Normalized by area correlation coefficients were slightly smaller but still statistically significant. Thus, excluding the influence of moderate reductions in overall cerebellar size (i.e., absolute sizes of the cerebellum), it can be asserted that fractal dimensions themselves had statistically significant associations with age.

When comparing correlation coefficients between studied parameters and age in males and females (Table 3), it is noticeable that the correlation relationships were somewhat stronger in males, suggesting more pronounced age-related changes. We calculated linear regression equations characterizing the age dynamics of cerebellar parameters in males and females (Fig. 4, Fig. 5). Comparing these equations, no statistically significant differences between males and females were found ($p > 0.05$).

4. Discussion

In this cross-sectional study, we conducted a comprehensive morphometric investigation of cerebellar aging, combining two morphometric approaches: conventional morphometry based on

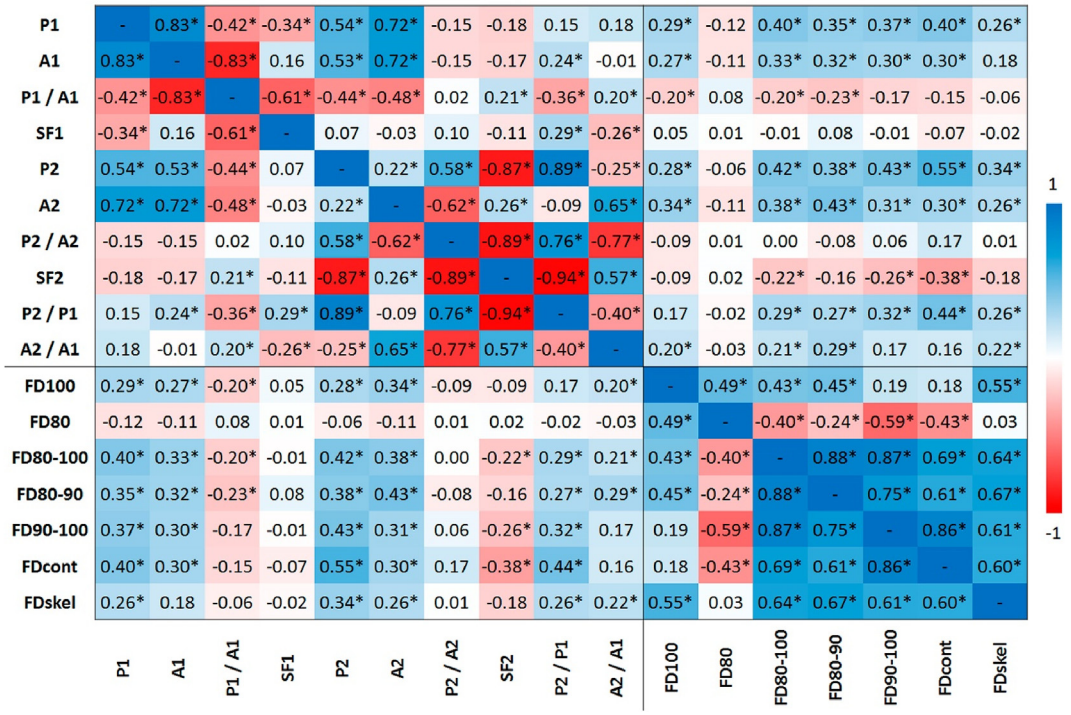

Fig. 3. Correlations between morphometric parameters of the cerebellar vermis; * – $p < 0.05$.

Table 3
Correlations between morphometric parameters of the cerebellar vermis and age.

Parameter	Total		Males		Females	
	R	$R_{N(A1)}$	R	$R_{N(A1)}$	R	$R_{N(A1)}$
P1	−0.344*	−0.004	−0.414*	−0.100	−0.238	0.191
A1	−0.413*	–	−0.479*	–	−0.366*	–
P1/A1	0.348*	0.009	0.393*	−0.152	0.312*	0.070
SF1	−0.110	−0.048	−0.162	0.070	−0.086	−0.088
P2	−0.239*	−0.025	−0.405*	−0.102	−0.050	0.096
A2	−0.352*	−0.085	−0.380*	−0.053	−0.342*	−0.112
P2/A2	0.041	−0.024	−0.177	−0.176	0.268	0.157
SF2	0.073	0.002	0.310*	0.158	−0.174	−0.162
P2/P1	−0.113	−0.016	−0.315*	−0.085	0.091	0.068
A2/A1	−0.043	−0.051	0.096	0.028	−0.173	−0.137
FD100	−0.098	0.016	−0.220	−0.081	−0.029	0.078
FD80	0.391*	0.382*	0.421*	0.422*	0.368*	0.356*
FD80-100	−0.448*	−0.361*	−0.596*	−0.497*	−0.296*	−0.227
FD80-90	−0.424*	−0.337*	−0.530*	−0.382*	−0.324*	−0.274*
FD90-100	−0.531*	−0.469*	−0.591*	−0.517*	−0.489*	−0.433*
FDskel	−0.251*	−0.199*	−0.297	−0.270	−0.216	−0.148
FDcont	−0.419*	−0.338*	−0.544*	−0.457*	−0.254	−0.189

Notes: Independent variable – age; R – conventional Spearman's rank correlation coefficient; $R_{N(A1)}$ – Spearman's rank correlation coefficient normalized by area A1; * – $p < 0.05$.

"classical" Euclidean geometry and the relatively new but promising fractal geometry approach. Despite the extensive exploration of aging patterns in the cerebral hemispheres through fractal analysis in previous studies,[26–30] it is notable that the investigation into cerebellar aging has not received deserved attention in the context of fractal analysis. Therefore, our aim was to provide a comprehensive analysis of fractal dimensions of the cerebellum obtained from conventional diagnostic MRI brain images. This allowed us to assess the vulnerability of cerebellar fractal dimensions to age-related changes and determine the dynamics of fractal dimension values throughout adulthood.

The results of the present study have shown that fractal dimension values demonstrated higher correlations with age compared to parameters derived from Euclidean geometry. The most pronounced age-related changes were observed in the values of FD80-100, FD80-90, and FD90-100, which represent approximated fractal dimensions for the overall cerebellar cortex, its granular, and molecular layers, respectively. Our findings align with studies by other authors who identified a decrease in fractal dimensions of the cerebral cortex and its surfaces (contours) during normal aging[26–28] and in Alzheimer's disease.[33,34]

The age-related reduction in approximated fractal dimensions of the cerebellar cortex can be attributed to decrease in the cortical thickness and simplification of the cortical spatial configuration, leading to its smoothing. This is supported by the significant decrease in the values of the fractal dimension of the contour (FDcont) and the fractal dimension of the digital skeleton (FDskel), which reflect the features of cerebellar structural complexity and the convolutedness of its surface, excluding the thickness of the cortex and its layers. However, fractal dimensions of the cortex and its layers exhibited stronger age-related correlation relationships than the fractal dimensions of the contour and skeleton, indicating

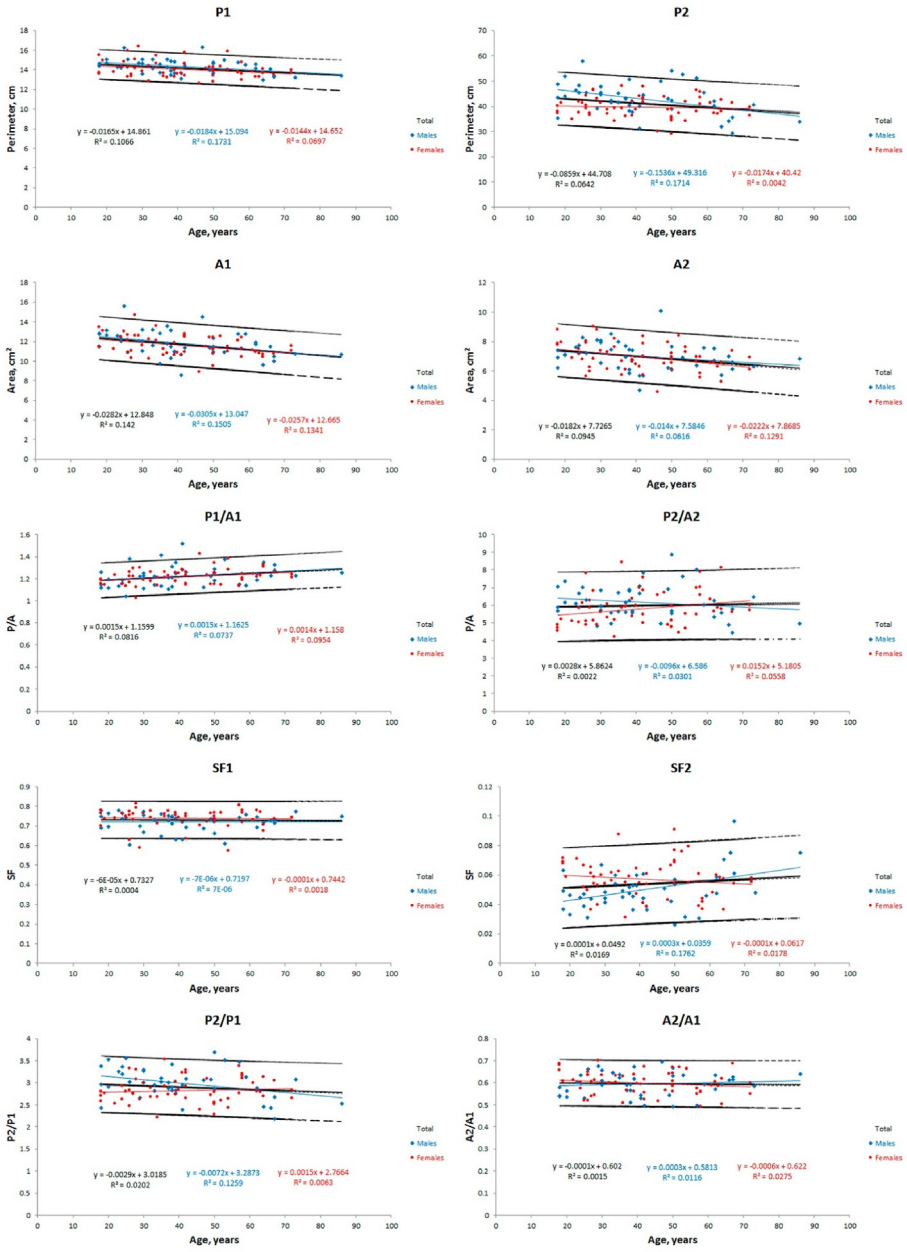

Fig. 4. Age dynamics and 95% confidence intervals of morphometric parameters derived from Euclidean geometry.

the influence of the first factor – a reduction in cortical thickness. Notably, the approximated fractal dimension of the molecular layer showed the strongest correlation with age. This can be attributed to the significant age-related loss of Purkinje cells,[17] whose dendritic trees form the basis of the molecular layer of the cerebellar cortex; therefore, the significant loss of Purkinje cells may contribute to a reduction in the thickness and fractal dimension of the molecular layer.

The approximated fractal dimension of the overall cerebellar tissue, FD100, did not exhibit significant age-related changes. Based on this finding, we can infer that despite a significant reduction in absolute sizes (measured by areas A1 and A2), the cerebellum does not undergo significant changes in the degree of space filling by overall cerebellar tissue.

Unlike the approximated fractal dimensions of the cortex and its contour, FD80, considered an approximated fractal dimension of the white matter, did not decrease; instead, it increased with age. In our previous study of cadaveric cerebella,[51] we determined the fractal dimension of the cerebellar white matter which significantly decreased with age. Such contradictory results can be explained by several factors. In our study conducted on cadaveric specimens, we had the opportunity to examine high-resolution images, visualizing even the smallest branches of the white matter within the folia. We believe that the thinning and shortening of these smallest branches primarily account for the strong negative correlation of the fractal dimension of the white matter with age. When examining MRI images, these branches within the folia are virtually unvisualized due to the limited capabilities of the MRI scanner, allowing only the study of the configuration of the main branches of the white matter. Therefore, we consider FD80 not as true but as an approximated fractal dimension of the white matter. Considering that segmentation with an intensity threshold of 80 reveals the major (largest) branches of the white matter, which are well visualized on MRI images, it would be logical to expect either the absence of age-related changes or a weak negative correlation with age. Why then did the values of FD80 significantly increase with age? We assume that this is due to age-related densification and water loss in cerebellar tissue. Thus, the densified and less hydrated areas of the cortex adjacent to the white matter branches are included in the silhouettes of the white matter

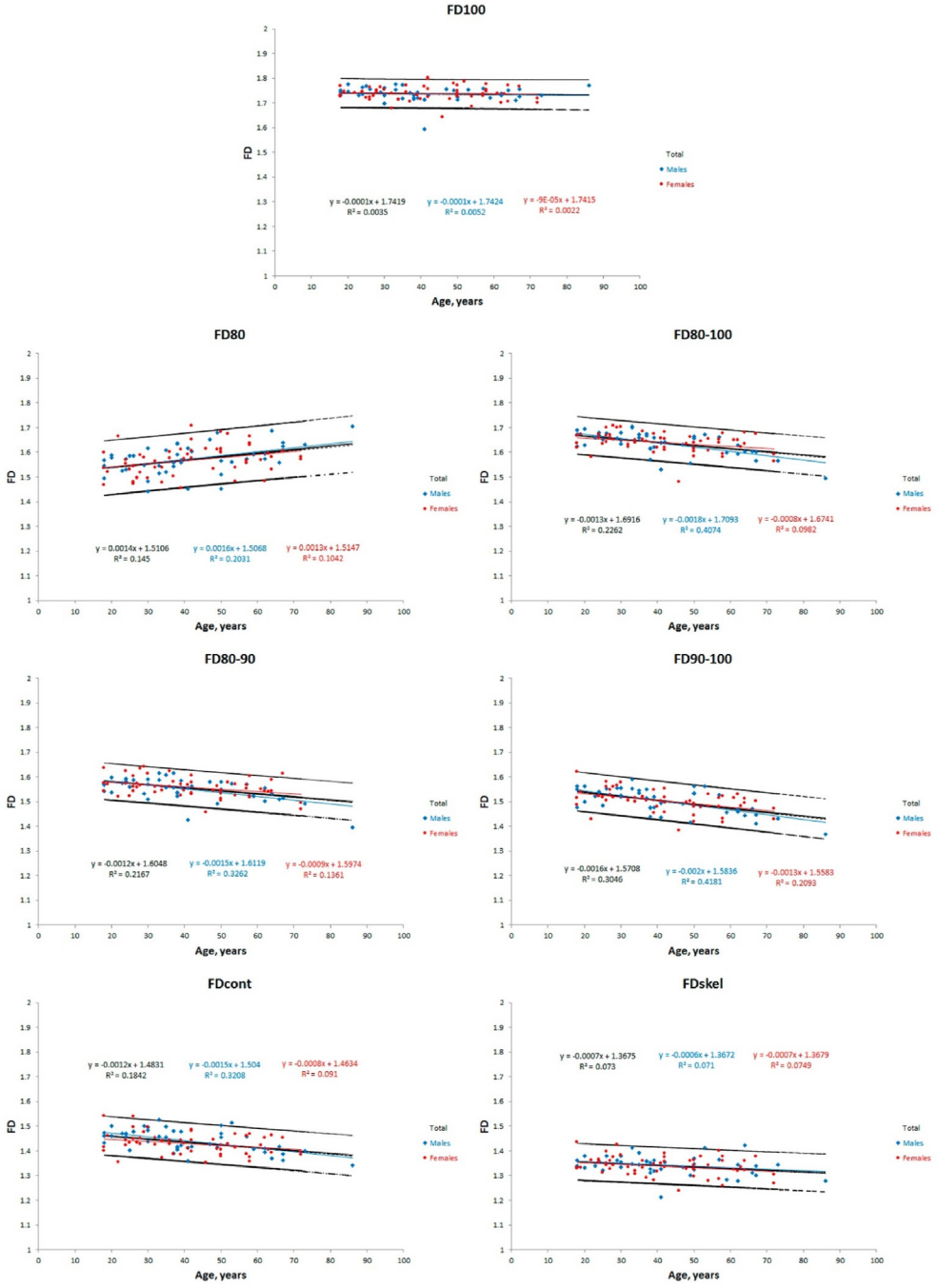

Fig. 5. Age dynamics and 95% confidence intervals of fractal dimension (FD) values.

during segmentation with an intensity threshold of 80, which accounts for the increase in FD80.

This factor may also contribute to the age-associated decrease in the cortical fractal dimensions FD80-100, FD80-90, and FD90-100. However, considering that FDcont also decreases during aging (while not directly depending on the intensity of cerebellar tissue components), it suggests that the intensity distribution of the cerebellar tissue is not the sole factor influencing the decline of approximated cortical fractal dimensions. The cortical structural and configuration changes may also significantly impact the age-related decline in the assessed parameters.

An alternative approximated fractal dimension of cerebellar white matter is FDskel. Skeletonization, an additional image pre-processing procedure, creates a digital skeleton inside the image, replicating the tree-like configuration of branched white matter forming the "framework" of the cerebellar cortex. This pre-processing method has its advantages as it is not dependent on the densification of cerebellar tissue. FDskel demonstrated a moderate decrease throughout adulthood, in contrast to FD80.

Comparing the age-related changes in the fractal dimensions of cerebellum and cerebral hemispheres, we should note that the cerebrum exhibited a more pronounced age-related decline: the correlation of average fractal dimension of cerebral surface with age identified in the same sample as in the present study was $R = -0.709$ (compared to the strongest correlation of cerebellar FD90-100 $R = -0.531$).[46] This assumption is supported by findings by C.R. Madan and E.A. Kensinger ($R = -0.732$ and $R = -0.719$, for the fractal dimension of the overall cerebral cortex and pial surface, respectively).[28]

Among the parameters derived from Euclidean geometry, the area and perimeter values exhibited the strongest correlations with age (although still weaker compared to fractal dimensions). The correlation coefficient values for the cerebellar vermis cross-sectional areas with age obtained in our study ($R = -0.413$, for area A1, and $R = -0.352$, for area A2) fall within the range of values reported by other researchers. For instance, in the research conducted by Murshed K.A. et al. ($N = 120$, age range 13–77 years), there was no significant change in the vermis area in males (R varied from −0.031 to 0.005) and a weak correlation with age in females (R varied from −0.329 to 0.154).[19] The study by Raz N. et al. ($N = 29$, age range 18–78 years) identified a moderately strong negative correlation between the vermis cross-sectional area and age ($R = -0.54$).[20] In the study by Serati M. et al. ($N = 38$, mean age 45.3 ± 9.6 years), it was found that the volume of the cerebellar vermis was weakly negatively correlated with age ($R = -0.22$ in males and $R = -0.17$ in females).[21] The differences in obtained R values can be explained by the limited size and heterogeneity of samples, as well as different age ranges.

The influence of sex is a potential factor affecting age-related changes in the studied morphometric parameters. The present study found that several parameters derived from Euclidean geometry, particularly those representing absolute sizes, were higher in males. This finding aligns with the generally larger cerebellum and brain sizes observed in males. However, the fractal dimension values did not differ significantly between males and females, suggesting that male and female cerebella, despite differing in absolute size, can exhibit the same degree of structural complexity. When examining the correlation coefficients between age and the studied parameters, other researchers have reported diverse changes in Euclidean geometry-derived parameters between males and females.[19,21] In the present study, the relationships were slightly stronger in males, indicating that age-related changes in cerebellar structure may be more pronounced in males. Despite this, the linear regression analyses did not reveal any statistically significant differences between the age-related dynamics of cerebellar parameters in males and females. This suggests that while there may be subtle gender-related differences in specific cerebellar metrics, the overall trajectory of cerebellar aging is comparable across genders.

When comparing fractal analysis and Euclidean geometry-based morphometry in studies of the cerebellum, particularly in the context of cerebellar aging, it is important to recognize that both methods have distinct advantages and disadvantages.

Euclidean geometry-based morphometry is widely utilized in neuroimaging studies due to its simplicity and robustness in the quantitative assessment of various brain structures, including the cerebellum. This approach focuses on measurable geometric properties such as area, perimeter, and volume, which characterize absolute sizes.[17–24] These properties are relatively straightforward to calculate and interpret, making Euclidean morphometry widely applicable in both clinical and research settings. The Euclidean geometry-based approach offers an assessment of linear changes in absolute cerebellar sizes. However, the absolute size of the cerebellum varies significantly among individuals due to differences in overall brain size, which may impact the age-related associations between Euclidean geometry-based parameters and age. Moreover, these measures are more suitable for assessing structures with geometrically simple shapes. Given that the cerebellum exhibits one of the highest degrees of spatial and structural complexity among brain structures, it can be inferred that Euclidean geometry alone cannot comprehensively assess such an intricate structure. Consequently, these parameters may not fully capture the intricate alterations that accompany aging, as indicated by the weaker correlations with age observed in our study.

On the other hand, fractal analysis has demonstrated higher sensitivity to age-related changes in the cerebellum. It is particularly attuned to subtle changes in cerebellar tissue that may not be captured by the Euclidean geometry-based approach, such as alterations in cerebellar structural complexity, space-filling capacity, convolutedness, and cortical thickness. In contrast to the Euclidean geometry-based approach, fractal analysis assesses non-linear changes in cerebellar structure, rather than merely linear changes in absolute cerebellar sizes. As shown in the present study, even after normalization for absolute sizes (specifically, cross-sectional area), fractal dimensions still exhibit age-related changes. Therefore, fractal analysis can be considered an informative and sensitive approach, particularly promising in the context of cerebellar aging studies and in differentiating normal aging from pathological conditions. However, the application of fractal analysis is associated with some challenges. One of the main challenges is its dependency on MRI image quality and resolution; the subtle and intricate patterns of cerebellar tissue texture must be clear and free of artifacts. Fractal analysis of the cerebellum requires the development of specialized image segmentation methods, which may need adjustments for different MRI sequences. Additionally, fractal analysis cannot assess linear changes in absolute cerebellar sizes, which also offer important information.

The primary limitation of this study was the limited clarity of the conventional diagnostic MRI images utilized. Therefore, we decided to determine not the true, but rather approximated values of the fractal dimensions of cerebellar tissue components. However, these approximations offer valuable insights into the sensitivity of fractal geometry methods to age-related changes and the presence of texture alterations in the cerebellum associated with aging. It is important to note that all MRI images investigated in this study were obtained using the same MRI scanner with the same imaging protocol.

5. Conclusion

This study has demonstrated the effectiveness of fractal analysis in detecting and quantitatively characterizing age-related changes in the cerebellum. The more pronounced age-related changes observed in fractal dimensions suggest a prevalence of alterations in the spatial configuration and texture of cerebellar tissue compared to less pronounced changes in absolute cerebellar sizes. Notably, the approximated fractal dimensions of the cerebellar cortex exhibited the strongest associations with normal aging, indicating their potential as sensitive MRI biomarkers. These findings underscore the practical value of fractal dimensions in the quantitative assessment of cerebellar changes in both normal and pathological aging, offering a promising tool for clinical application in diagnosing and tracking cerebellar involvement in various neurological conditions.

Ethics approval and consent to participate

The study was conducted in accordance with the Declaration of Helsinki, and approved by the Commission on Ethics and Bioethics of Kharkiv National Medical University (minutes of the meeting of the Commission on Ethics and Bioethics of KhNMU No. 10 of Nov. 7, 2018) for studies involving humans. Written informed consent has been obtained from the participants of the study.

Authorship Statement

Nataliia Maryenko: Writing – original draft, Visualization, Methodology, Investigation, Formal analysis, Data curation, Conceptualization. **Oleksandr Stepanenko:** Writing – review & editing, Validation, Supervision, Project administration, Methodology, Conceptualization.

Declaration of Competing Interests

The authors declare that they have no known competing financial interests or personal relationships that could have appeared to influence the work reported in this paper.

Acknowledgments

The authors would like to express their sincere gratitude to the participants of this study, without whom this research would not have been possible.

References

1. Koziol LF, Budding D, Andreasen N, et al. Consensus paper: the cerebellum's role in movement and cognition. *Cerebellum*. 2014;13(1):151–177. https://doi.org/10.1007/s12311-013-0511-x.
2. Schmahmann JD. The cerebellum and cognition. *Neurosci Lett*. 2019;688:62–75. https://doi.org/10.1016/j.neulet.2018.07.005.
3. MacLullich AM, Edmond CL, Ferguson KJ, et al. Size of the neocerebellar vermis is associated with cognition in healthy elderly men. *Brain Cognit*. 2004;56(3):344–348. https://doi.org/10.1016/j.bandc.2004.08.001.
4. Bernard JA, Seidler RD. Moving forward: age effects on the cerebellum underlie cognitive and motor declines. *Neurosci Biobehav Rev*. 2014;42:193–207. https://doi.org/10.1016/j.neubiorev.2014.02.011.
5. Bernard JA. Don't forget the little brain: a framework for incorporating the cerebellum into the understanding of cognitive aging. *Neurosci Biobehav Rev*. 2022;137:104639. https://doi.org/10.1016/j.neubiorev.2022.104639.
6. Ramanoël S, Durteste M, Perot V, Habas C, Arleo A. An appraisal of the role of the neocerebellum for spatial navigation in healthy aging. *Cerebellum*. 2023;22(2):235–239. https://doi.org/10.1007/s12311-022-01389-1.
7. Arleo A, Bareš M, Bernard JA, et al. Consensus paper: cerebellum and ageing. *Cerebellum*. 2024;23(2):802–832. https://doi.org/10.1007/s12311-023-01577-7.
8. Romero JE, Coupe P, Lanuza E, Catheline G, Manjón JV. Alzheimer's Disease Neuroimaging Initiative. Toward a unified analysis of cerebellum maturation and aging across the entire lifespan: a MRI analysis. *Hum Brain Mapp*. 2021;42(5):1287–1303. https://doi.org/10.1002/hbm.25293.
9. Schmahmann JD, Doyon J, McDonald D, et al. Three-dimensional MRI atlas of the human cerebellum in proportional stereotaxic space. *Neuroimage*. 1999;10(3 Pt 1):233–260. https://doi.org/10.1006/nimg.1999.0459.
10. Diedrichsen J, Balsters JH, Flavell J, Cussans E, Ramnani N. A probabilistic MR atlas of the human cerebellum. *Neuroimage*. 2009;46(1):39–46. https://doi.org/10.1016/j.neuroimage.2009.01.045.
11. Mormina E, Petracca M, Bommarito G, Piaggio N, Cocozza S, Inglese M. Cerebellum and neurodegenerative diseases: beyond conventional magnetic resonance imaging. *World J Radiol*. 2017;9(10):371–388. https://doi.org/10.4329/wjr.v9.i10.371.
12. Gellersen HM, Guo CC, O'Callaghan C, Tan RH, Sami S, Hornberger M. Cerebellar atrophy in neurodegeneration-a meta-analysis. *J Neurol Neurosurg Psychiatry*. 2017;88(9):780–788. https://doi.org/10.1136/jnnp-2017-315607.
13. Öz G, Harding IH, Krahe J, Reetz K. MR imaging and spectroscopy in degenerative ataxias: toward multimodal, multisite, multistage monitoring of neurodegeneration. *Curr Opin Neurol*. 2020;33(4):451–461. https://doi.org/10.1097/WCO.0000000000000834.
14. Huang YP, Tuason MY, Wu T, Plaitakis A. MRI and CT features of cerebellar degeneration. *J Formos Med Assoc*. 1993;92(6):494–508.
15. Mascalchi M, Vella A. Neuroimaging applications in chronic ataxias. *Int Rev Neurobiol*. 2018;143:109–162. https://doi.org/10.1016/bs.irn.2018.09.011.
16. Arruda WO, Meira AT, Ono SE, et al. Volumetric MRI changes in spinocerebellar ataxia (SCA3 and SCA10) patients. *Cerebellum*. 2020;19(4):536–543. https://doi.org/10.1007/s12311-020-01137-3.
17. Shyian D, Galata D, Potapov S, Gargin V. Peculiarities of the cerebellum nuclei in aged persons. *Georgian Med News*. 2016;253:110–115.
18. Hayakawa K, Konishi Y, Matsuda T, et al. Development and aging of brain midline structures: assessment with MR imaging. *Radiology*. 1989;172(1):171–177. https://doi.org/10.1148/radiology.172.1.2740500.
19. Murshed KA, Ziylan T, Seker M, Cicekcibasi AE, Acikgozoglu S. Morphometric assessment of brain stem and cerebellar vermis with midsagittal MRI: the gender differences and effects of age. *Neuroanatomy*. 2003;2:35–38.
20. Raz N, Torres IJ, Spencer WD, White K, Acker JD. Age-related regional differences in cerebellar vermis observed in vivo. *Arch Neurol*. 1992;49(4):412–416. https://doi.org/10.1001/archneur.1992.00530280106030.
21. Serati M, Delvecchio G, Orsenigo G, et al. Potential gender-related aging processes occur earlier and faster in the vermis of patients with bipolar disorder: an MRI study. *Neuropsychobiology*. 2017;75(1):32–38. https://doi.org/10.1159/000477967.
22. Yu T, Korgaonkar MS, Grieve SM. Gray matter atrophy in the cerebellum-evidence of increased vulnerability of the crus and vermis with advancing age. *Cerebellum*. 2017;16(2):388–397. https://doi.org/10.1007/s12311-016-0813-x.
23. Han S, An Y, Carass A, Prince JL, Resnick SM. Longitudinal analysis of regional cerebellum volumes during normal aging. *Neuroimage*. 2020;220:117062. https://doi.org/10.1016/j.neuroimage.2020.117062.
24. Stalter J, Yogeswaran V, Vogel W, Sörös P, Mathys C, Witt K. The impact of aging on morphometric changes in the cerebellum: a voxel-based morphometry study. *Front Aging Neurosci*. 2023;15:1078448. https://doi.org/10.3389/fnagi.2023.1078448.
25. Mandelbrot BB. *The Fractal Geometry of Nature*. San Francisco: W.H. Freeman and Company; 1982.
26. Podgórski P, Bladowska J, Sasiadek M, Zimny A. Novel volumetric and surface-based magnetic resonance indices of the aging brain - does male and female brain age in the same way? *Front Neurol*. 2021;12:645729. https://doi.org/10.3389/fneur.2021.645729.
27. Kalmanti E, Maris TG. Fractal dimension as an index of brain cortical changes throughout life. *In Vivo*. 2007;21(4):641–646.
28. Madan CR, Kensinger EA. Cortical complexity as a measure of age-related brain atrophy. *Neuroimage*. 2016;134:617–629. https://doi.org/10.1016/j.neuroimage.2016.04.029.
29. Farahibozorg S, Hashemi-Golpayegani SM, Ashburner J. Age- and sex-related variations in the brain white matter fractal dimension throughout adulthood: an MRI study. *Clin Neuroradiol*. 2015;25(1):19–32. https://doi.org/10.1007/s00062-013-0273-3.
30. Zhang L, Dean D, Liu JZ, Sahgal V, Wang X, Yue GH. Quantifying degeneration of white matter in normal aging using fractal dimension. *Neurobiol Aging*. 2007;28(10):1543–1555. https://doi.org/10.1016/j.neurobiolaging.2006.06.020.
31. Esteban FJ, Sepulcre J, de Mendizábal NV, et al. Fractal dimension and white matter changes in multiple sclerosis. *Neuroimage*. 2007;36(3):543–549. https://doi.org/10.1016/j.neuroimage.2007.03.057.
32. Esteban FJ, Sepulcre J, de Miras JR, et al. Fractal dimension analysis of grey matter in multiple sclerosis. *J Neurol Sci*. 2009;282(1-2):67–71. https://doi.org/10.1016/j.jns.2008.12.023.
33. King RD, George AT, Jeon T, et al, the Alzheimer's Disease Neuroimaging Initiative. Characterization of atrophic changes in the cerebral cortex using fractal dimensional analysis. *Brain Imaging Behav*. 2009;3(2):154–166. https://doi.org/10.1007/s11682-008-9057-9.
34. King RD, Brown B, Hwang M, Jeon T, George AT. Alzheimer's Disease Neuroimaging Initiative. Fractal dimension analysis of the cortical ribbon in mild Alzheimer's disease. *Neuroimage*. 2010;53(2):471–479. https://doi.org/10.1016/j.neuroimage.2010.06.050.
35. Rybaczuk M, Kedzia A, Błaszczyk E. Fractal description of cerebellum surface during fetal period. *Folia Morphol (Wars)*. 1996;55(4):434–436.
36. Rybaczuk M, Kedzia A. Fractal analysis of adults cerebellum surface NMR observations. *Folia Morphol (Wars)*. 1996;55(4):431–433.
37. Liu JZ, Zhang LD, Yue GH. Fractal dimension in human cerebellum measured by magnetic resonance imaging. *Biophys J*. 2003;85(6):4041–4046. https://doi.org/10.1016/S0006-3495(03)74817-6.
38. Wu YT, Shyu KK, Jao CW, et al. Fractal dimension analysis for quantifying cerebellar morphological change of multiple system atrophy of the cerebellar type (MSA-C). *Neuroimage*. 2010;49(1):539–551. https://doi.org/10.1016/j.neuroimage.2009.07.042.
39. Akar E, Kara S, Akdemir H, Kırış A. Fractal dimension analysis of cerebellum in Chiari Malformation type I. *Comput Biol Med*. 2015;64:179–186. https://doi.org/10.1016/j.compbiomed.2015.06.024.
40. Akar E, Kara S, Akdemir H, Kırış A. 3D structural complexity analysis of cerebellum in Chiari malformation type I. *Med Biol Eng Comput*. 2017;55(12):2169–2182. https://doi.org/10.1007/s11517-017-1661-7.
41. Akar E, Kara S, Akdemir H, Kırış A. Fractal analysis of MR images in patients with chiari malformation:The importance of preprocessing. *Biomed Signal Process Control*. 2017;31:63–70. https://doi.org/10.1016/j.bspc.2016.07.005.
42. Marzi C, Ciulli S, Giannelli M, et al. Structural complexity of the cerebellum and cerebral cortex is reduced in spinocerebellar ataxia type 2. *J Neuroimaging*. 2018;28(6):688–693. https://doi.org/10.1111/jon.12534.
43. Zhao G, Walsh K, Long J, Gui W, Denisova K. Reduced structural complexity of the right cerebellar cortex in male children with autism spectrum disorder. *PLoS One*. 2018;13(7):e0196964. https://doi.org/10.1371/journal.pone.0196964.
44. Maryenko N, Stepanenko O. Characterization of white matter branching in human cerebella: quantitative morphological assessment and fractal analysis of skeletonized MR images. *Biomed Research and Therapy*. 2021;8(5):4345–4357. https://doi.org/10.15419/bmrat.v8i5.673.
45. Maryenko N, Stepanenko O. Fractal dimension of external linear contour of human cerebellum (magnetic resonance imaging study). *Reports of Morphology*. 2021;27(2). https://doi.org/10.31393/morphology-journal-2021-27(2)-03, 16-2.
46. Maryenko N, Stepanenko O. Quantitative characterization of age-related atrophic changes in cerebral hemispheres: a novel “contour smoothing” fractal analysis method. *Trans Research in Anatomy*. 2023;33:100263. https://doi.org/10.1016/j.tria.2023.100263.
47. Larsell O, Jansen J. *The Comparative Anatomy and Histology of the Cerebellum*. Minneapolis: University of Minnesota Press; 1972.
48. Underwood EE. *Quantitative Stereology*. London: Addison-Wesley; 1970.
49. Schneider CA, Rasband WS, Eliceiri KW. NIH Image to ImageJ: 25 years of image analysis. *Nat Methods*. 2012;9(7):671–675. https://doi.org/10.1038/nmeth.2089.
50. Karperien AL, Jelinek HF. Box-counting fractal analysis: a primer for the clinician. *Adv Neurobiol*. 2024;36:15–55. https://doi.org/10.1007/978-3-031-47606-8_2.
51. Stepanenko AY, Maryenko NI. Fractal analysis of the human cerebellum white matter. *World of medicine and biology*. 2017;3(61):145–149. https://doi.org/10.26724/2079-8334-2017-3-61-145-149 [In Russian].